Probabilistic assessment of uncertainties in induced seismic potential of the San Juan Basin CarbonSAFE Phase III deep saline carbon sequestration site

Kevin L. McCormack[1], Tom Bratton[2], Ting Chen[3], and Brian McPherson[1]

[1]University of Utah
[2]Tom Bratton LLC
[3]Los Alamos National Laboratory

November 25, 2022

Abstract

Although geologic carbon sequestration projects have yet to induce – or may never induce – a damaging earthquake, experiences from other deep injection industries such as hydraulic fracturing, enhanced geothermal systems, and saltwater disposal suggest that effective quantitative seismic risk assessment is necessary for deep saline carbon capture and sequestration (CCS) projects. One such imminent CCS project is the San Juan Basin CarbonSAFE Phase III program. The study detailed in this paper utilizes Monte Carlo probabilistic geomechanical analyses combined with observations of the geological and operational parameters of the San Juan Basin site and suggests that this project is of low induced seismic risk. The primary analysis is split into four sections. First, we assessed the literature for faults and past seismicity, and at least five faulting scenarios are directly relevant. Second, we developed and calibrated an integrated earth model for the project site. Third, we performed Monte Carlo simulations that considered reasonable uncertainties of the geomechanical parameters. Only the Hogback flexural faulting scenario presented high Coulomb failure functions, but fourth, we determined the risk to be low based on the combined lack of historical seismicity, the geological framework of the flexural faults, and the presence of saltwater injection at the same depth as the proposed supercritical carbon dioxide injection. The most sensitive parameters in the geomechanical calculations were the fault dip and the coefficient of friction. The least sensitive were the fault strike and the orientation of the maximum horizontal principal stress.

Probabilistic assessment of uncertainties in induced seismic potential of the San Juan Basin CarbonSAFE Phase III deep saline carbon sequestration site

Kevin L. McCormack[1], Tom Bratton[2], Ting Chen[3], and Brian McPherson[1]

[1]Energy and Geoscience Institute – University of Utah.

[2]Tom Bratton L.L.C.

[3]Los Allamos National Lboratory.

Corresponding author: Kevin L. McCormack (kmccormack@egi.utah.edu)

Key Points:

- We do not anticipate medium- to large-scale rupture in the San Juan Basin related to the injection of supercritical carbon dioxide from the CarbonSAFE Phase III project.
- The results of the geomechanical simulations must be contextualized within the operational parameters of the basin, the seismic history, and the geologic framework.
- The geomechanical simulations are most sensitive to the coefficient of friction and the dip of the faults.

Abstract

Although geologic carbon sequestration projects have yet to induce – or may never induce – a damaging earthquake, experiences from other deep injection industries such as hydraulic fracturing, enhanced geothermal systems, and saltwater disposal suggest that effective quantitative seismic risk assessment is necessary for deep saline carbon capture and sequestration (CCS) projects. One such imminent CCS project is the San Juan Basin CarbonSAFE Phase III program. The study detailed in this paper utilizes Monte Carlo probabilistic geomechanical analyses combined with observations of the geological and operational parameters of the San Juan Basin site and suggests that this project is of low induced seismic risk. The primary analysis is split into four sections. First, we assessed the literature for faults and past seismicity, and at least five faulting scenarios are directly relevant. Second, we developed and calibrated an integrated earth model for the project site. Third, we performed Monte Carlo simulations that considered reasonable uncertainties of the geomechanical parameters. Only the Hogback flexural faulting scenario presented high Coulomb failure functions, but fourth, we determined the risk to be low based on the combined lack of historical seismicity, the geological framework of the flexural faults, and the presence of saltwater injection at the same depth as the proposed supercritical carbon dioxide injection. The most sensitive parameters in the geomechanical calculations were the fault dip and the coefficient of friction. The least sensitive were the fault strike and the orientation of the maximum horizontal principal stress.

Plain Language Summary

Injection projects have been shown sometimes to cause damaging earthquakes. Therefore, we have identified potentially problematic faults in the San Juan Basin, and we have performed detailed analyses of these faults to determine whether they are likely to host a large earthquake. Only one set of faults that we analyzed is potentially hazardous. When contextualized in the operational parameters of the basin, the seismic history, and the geologic framework of the faulting system, however, that hazard becomes minimal.

1 Introduction

The San Juan Basin CarbonSAFE Phase III project is a deep saline carbon sequestration project that will inject between 6-7 million metric tons of supercritical carbon dioxide per year over a period of 12-20 years. The primary target formation is the Entrada sandstone, although other reservoirs and seals in the sedimentary column will allow for stacked storage. Large-scale injection projects such as this, be they saltwater disposal (e.g. Walsh and Zoback, 2015; Rubinstein and Mahani, 2015; Lagenbruch and Zoback, 2017; Hinks et al., 2018), enhanced geothermal systems (e.g. Grigoli et al., 2018; Ellsworth et al., 2019; Catalli et al., 2016; Mignan et al., 2015; McClure and Horne, 2011; Majer et al., 2007), carbon sequestration (e.g. Mazzoldi et al., 2012; White and Foxall, 2016; Vilarrasa et al., 2019; Nicol et al., 2011; Rutqvist et al., 2016), or hydraulic fracturing operations (e.g. Schultz et al., 2018; Davies et al., 2013; Warpinski et al., 2012; Shapiro and Dinske, 2009), have the ability to induce potentially damaging earthquakes and must be scrutinized for seismic hazards associated with the project. In addition to infrastructure damage, induced events at carbon sequestration sites also have the potential to denigrate the integrity of the caprock – at all scales of rupture. This study focuses on the potential for a damaging medium- to large-scale rupture.

Carbon sequestration operations have been ongoing since 1996 with the first commercial scale project in the Sleipner oil field in the North Sea (Torp and Gale, 2004). Despite this long history, carbon sequestration projects have yet to induce a sizeable earthquake (White and Foxall, 2016; Vilarrasa et al., 2019). Three primary reasons are posited for this success in the deep saline setting. First, as supercritical carbon dioxide is injected into *in situ* brine, that carbon dioxide partially dissolves in the brine, reducing pressure. Therefore, the pressure in the formation decreases to less than that of the injection (Vilarrasa et al., 2019). Second, the lower viscosity and higher compressibility of carbon dioxide allows it to flow through the formation more easily than other fluid types, for instance, saltwater, and thus injection of carbon dioxide causes less pressure in the formation than equivalent injection of different fluid types (Krevor et al., 2012). Finally, the diligent work involved in choosing projects and sites that are low in both seismic hazard and risk cannot be discounted.

In this paper, we use novel geomechanical analyses along with analysis of past seismicity and operations in the basin to evaluate whether the San Juan Basin CarboSAFE Phase III site is of low induced seismic risk. The paper is split into four sections. First, we analyze available literature on faulting in the San Juan basin and past seismicity. Second, we briefly construct a one-dimensional geomechanical model. Third, we assess geomechanical properties of the basin and the bulk of the analysis utilizes probabilistic Mohr circles. And finally, we analyze the results in terms of existing operational data in the basin (specifically saltwater disposal), past seismicity, and analytical poroelastic calculations.

2 Methodology

2.1 Faults in the Basin and Past Seismicity

The first step in determining the seismic hazard was to assess what information about geologic faults had been published in the literature. The San Juan Basin is a relatively seismically quiescent sedimentary basin in the Four Corners region of the United States. Only thirty earthquakes in the basin of magnitude 2.5 or greater since 1966 are reported in the US Geological Survey's (USGS) database, including two events both estimated to be approximately moment magnitude of 5.0 (Figure 1). One occurred in 1966, and the other occurred in 1976. We used the hypocentral locations and magnitudes of these fifteen earthquakes to approximate the fault planes in two conjugate sets using critically stressed crust theory (Zoback, 2007). This method of determining fault planes is highly uncertain because it assumes that every fault that slipped was perfectly oriented to the stress field. Also, it offers no ability to differentiate between conjugate faults.

All but one of these faults are located within the crystalline basement. These faults are all far from the area of interest, which covers roughly 500 square miles in the northwestern part of the basin (Figure 1). Much of the fault mapping that has been performed from 2D seismic profiles in the basin indicate that most of the faults are in the basement domain (Taylor and Huffman, 1998; Majer et al., 2004). Taylor and Huffman (1998) identified two nearly perpendicular sets of normal faults in the basement, while Majer et al. (2004) identified a complicated series of faulting striking east-west. Evidence from several active seismic sources suggests there exists some faulting above the basement. It is not clear if these faults penetrate through the target formations such as the Entrada, Lower Morrison (Salt Wash), Bluff Sandstone, and their respective caprock layers for the San Juan Basin CarbonSAFE storage complex.

While most of the mapped faulting is believed to be normal faulting, Lorenz and Cooper (2001) indicated that blind thrust faults are present in the sedimentary cover. These are perhaps the result of Laramide reactivation of basement faults (Lorenz and Cooper, 2003; Craigg, 2001). Furthermore, outcrops throughout the San Juan basin exhibit fractures, indicating that discontinuities are present from basement to surface (Fassett and Boyce, 2005; Dart, 1992; Hart and Cooper, 2021). Outcrop fractures are mostly bed-bounded, but several throughgoing features that cut bedding planes are observed as well (Hart and Cooper, 2021). Faults and fractures identified at the surface cannot easily be extrapolated to depth where they could host a seismic event. Challenges of characterizing mapped faults in the basin include assumptions of critically stressed crust, low resolution in the basement of active seismic images, and the uncertainty of extrapolating outcrop data to depth. Thus, the seismic hazard is challenging to identify, and we therefore elected to employ a probabilistic approach. In total, we found five faults or sets of faults that we hypothesized might pose some risk to the project. These five sets of faults were: 1) Basement faults striking 35 degrees (Taylor and Huffman, 1998), 2) Basement faults striking 125 degrees (Taylor and Huffman, 1998), 3) flexural faults in the limb of the Hogback, 4) a vertical fault separating the limb of the Hogback from the rest of the basin, and 5) a set of faults mapped in the overlying Dakota sandstone (Lorenz and Cooper, 2001). These faulting scenarios will be discussed in more detail.

In addition to regional earthquakes identified by the USGS catalog, we examined other sources for seismicity in this region, including historical record (Sanford et al., 1981), data from the Earthscope USArray experiment (Astiz et al., 2014) and other seismic networks in the area (Sanford et al., 2002, 2006; Pursley et al., 2013). A total of approximately 1000 seismic events are found in the broader basin region, including some likely mining events from the USArray catalog. Most of these events exhibit magnitudes smaller than 3 and depths between 0 and 10 miles. Within the area of interest, there are six small events. The largest one was magnitude 2.2 and depth 1.1 miles. Two of the six events, including the largest one, fall in the region of the Hogback monocline, a region of interest for the induced seismicity potential of the CarbonSAFE project. These two events are analyzed in greater detail later.

The occurrence of the two magnitude 5.0 earthquakes in the USGS database indicates potential for larger events in the basin, albeit these two events occurred more than 50 miles from the proposed injection site. Furthermore, the quantity of events seen in the USArray dataset and additional seismic networks indicates that despite being relatively quiescent, the basin still hosts some degree of seismic activity. Figure 1 depicts the seismic events in relation to the seismic stations in the region and the proposed injection site. Most of the seismicity occurs significantly distantly from the site, and as the site is in the subhorizontal sedimentary layers of the inner basin, we see that the majority of the seismicity occurs in the structurally more complicated regions around the periphery of the basin. Also in Figure 1, the Hogback monocline is depicted along with the boundaries of the basin.

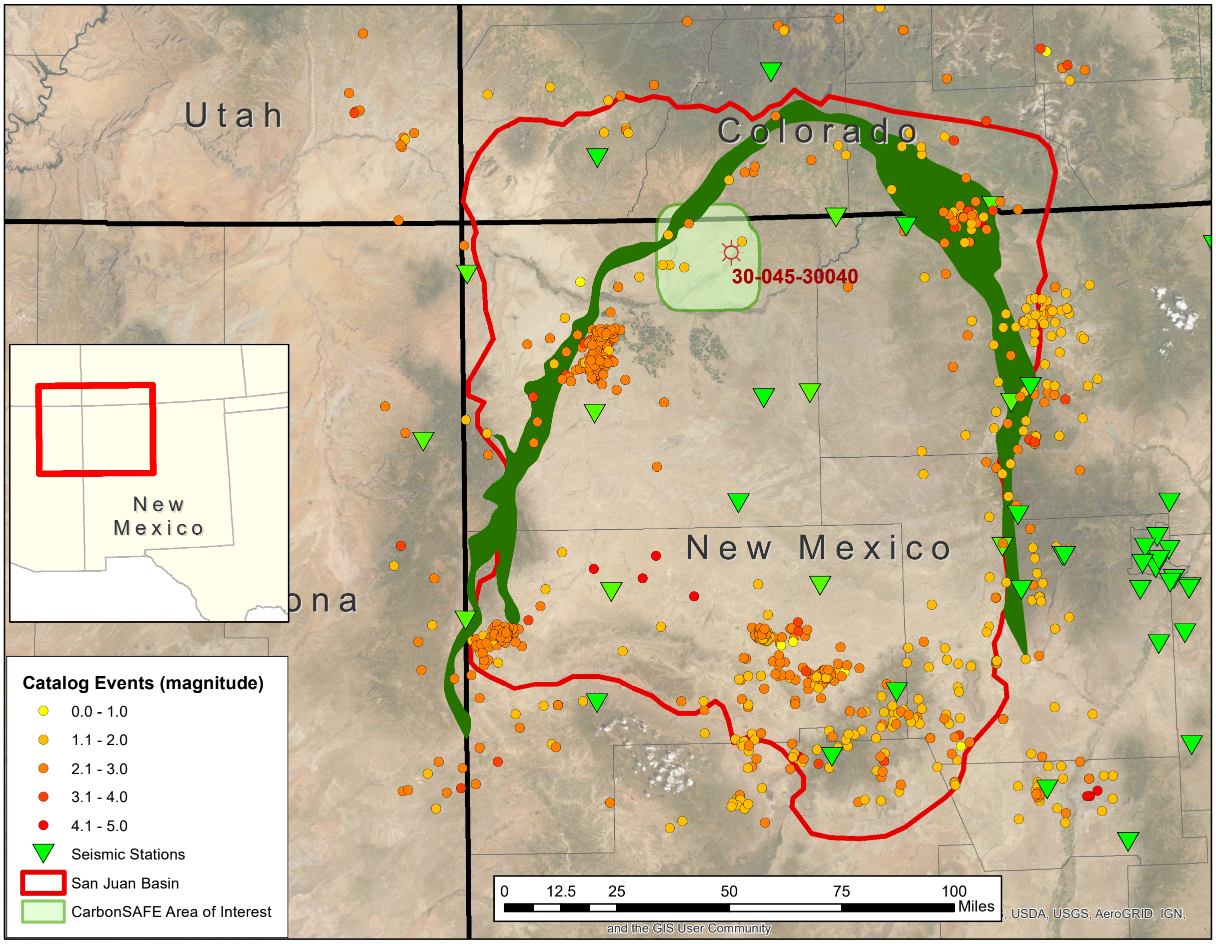

Figure 1: Map of the seismicity from roughly 60 years of USGS instrumentation and a short period of local instrumentation. There are a total of 1091 events. The dark green outline is the Hogback Monocline as interpreted from Lorenz and Cooper (2003). The 30-045-30040 well corresponds to the primary well used to create the integrated earth model (below).

2.2 Integrated Earth Model

The second step in this analysis is to identify the state of stress. Using petrophysical logs, we were able to create a one-dimensional integrated earth model (IEM). The purpose of an IEM is to provide a complete collection of input data required to run a geomechanical simulation. While the components of the earth model vary with the requirements of the geomechanical simulation, in general there are eight components to the IEM: 1) a framework model to characterize the structure of the formation including formation horizons and major faults, 2) a petrophysical model to quantify the lithology, porosity, water saturation, matrix permeability, and dynamic elastic moduli, 3) a stratigraphy model to characterize the stratigraphic column, load bearing facies, and natural and drilling induced fracture attributes, 4) a rock property model to characterize the static moduli, deformation, yield, and failure properties of the formation, 5) an overburden model to characterize the vertical loading, 6) a pore pressure model to quantify the pore pressure, 7) a stress orientation model to characterize the dip and azimuth of the far-field stresses, and finally 8) a stress magnitude model to quantify the horizontal loading on the formations. Figure 2 shows the eight components of the IEM and the typical sources of data to construct the individual models.

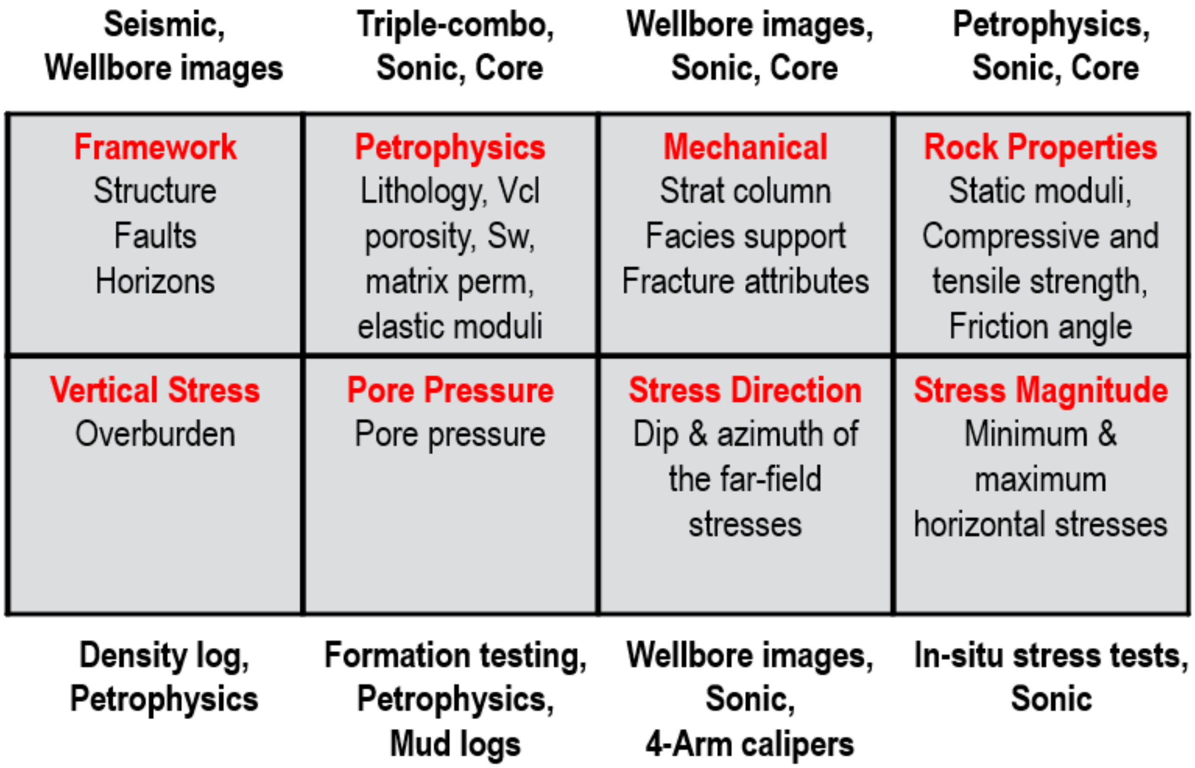

Figure 2: The components of an integrated earth model (inside the boxes) and typical sources of input data (outside of the boxes).

The petrophysical model was built considering 11 wells in the area of interest (light green area in Figure 1) and an additional 6 wells adjacent to that area. All wells were logged with triple-combo wireline tools, 8 wells have a P-wave velocity, and 3 wells have a S-wave velocity. The petrophysical model included a minimum of three minerals, quartz, calcite, and Illite, and two fluids, gas and water. The 30-045-30040 well of Figure 1 is the only well for which there was a shear log over the majority of the sedimentary column. Matrix permeability was computed using Herron's Geochemical algorithm (Herron, 1987), and the isotropic dynamic elastic moduli were computed using measured P-wave and S-wave velocities. The mechanical stratigraphy model was constructed using petrophysical cross plot methods (Herron et al., 1992).

Next, the rock properties model was built using standard geomechanical correlations. The static Young's modulus was derived from the Morales correlation (Morales et al., 1993), the unconfined compressive strength was derived from the Coates-Denoo correlation (Coates and Denoo, 1981), and the friction angle was derived from the Plumb correlation (Plumb, 1994). Following the rock properties model, the overburden model was constructed by integrating the measured bulk density from the surface to the depth of the pre-Cambrian basement. An exponential bulk density model was used in the top 300 feet where no bulk density measurement was made. In addition, a bulk density curve based on the petrophysical model is used in place of the measured bulk density in intervals of enlarged and rugose borehole where the measured bulk density is invalid.

The pore pressure model was constructed by integrating the fluid density from the surface to the deepest depth of interest. This estimate models the formations as hydrostatically pressured.

The far-field stress orientation is assumed perfectly vertical and horizontal. The direction of the maximum horizontal stress is adapted from the stress map reported in Lund Snee and Zoback (2020).

The stress magnitude model was constructed based on quantitative estimates of the mechanical behavior of each layer. In higher strength layers, where in-situ stresses are estimated to be less than the elastic limit of the layer, a standard linear elastic horizontal strain model was selected. In contrast, we applied a standard Mohr-Coulomb model to lower strength, critically stressed layers where the standard linear elastic model estimates the in-situ stresses to be greater than the confined compressive strength. An interpolated model was used for layers that are estimated to be greater than the elastic limit but less than the confined compressive strength of the critically stressed layers (Bratton and Soroka, 2018). The maximum horizontal stress was computed using the tectonic strain terms in the selected standard elastic horizontal strain model. The same tectonic imbalance computed from the linear elastic horizontal strain model was used in the critically stressed layers. The resultant IEM or stress profile (Figure 3) is predicated on several assumptions, but the Monte Carlo approach that we take is designed to account for many types of uncertainty.

The faulting regime (Figure 3) is clearly normal-faulting where S_v is greater than the two horizontal principal stresses, but more than that, the two horizontal principal stresses are nearly equal indicating that this is a radial normal-faulting regime. Radial normal faulting implies that the strike of the faults is relatively unimportant for whether they are critically stressed. This observation means all strikes of faults are potentially active, albeit there are also other factors that affect the shear and normal stresses resolved on the fault, especially the dip. Additionally, the stress state is very close to, if not crossing the frictional failure equilibrium line for the majority of the profile, which means that well-oriented faults are likely to slip. This is a common occurrence in most tectonic settings around the world (Townend and Zoback, 2000).

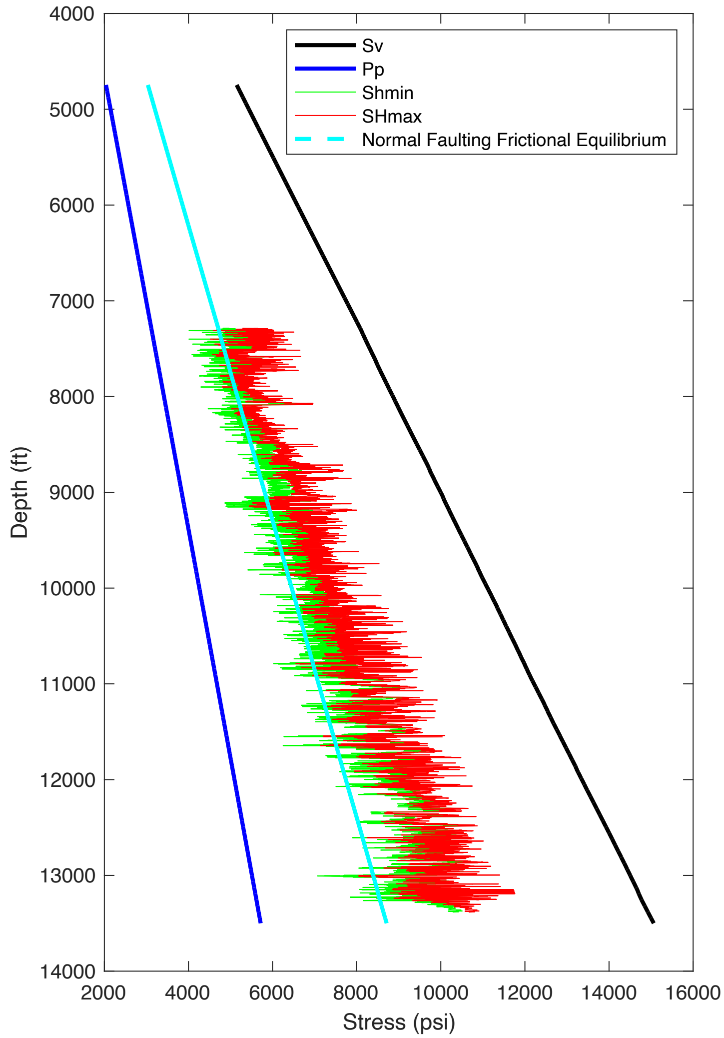

Figure 3: The stress profile obtained from the integrated earth model.

2.3 Geomechanical Simulations

Using the stress profile (Figure 3), we conduct a Mohr-Coulomb analysis on particular faults or sets of faults that we identified in the literature. Five systems are chosen for the completeness of the data available and the proximity to the proposed injection site. Two of these systems are both sets of basement faults from Taylor and Huffman (1998), one striking roughly 35 degrees and the other orthogonally at about 125 degrees. While these two sets of faults are not mapped specifically at the location of interest (light green area in Figure 1), they are present in all available seismic data, and thus for the sake of being conservative, we assume that these faults would have been mapped at the proposed site had data been available. The third faulting scenario that we will analyze is flexural faulting associated with the folding of the Hogback monocline. Some authors (Craigg, 2001; Lorenz and Cooper, 2001; Kelley, 1957) hypothesize that the hogback is a monocline without an associated fault, but Gorham et al. (1979) theorize that relatively high volumes of oil production along the monocline is due to flexural faulting, and indeed given the steep nature of the limb of the monocline of about 50 degrees (Craigg, 2001), we decided to account for the potential of some degree of flexural faulting. Therefore, for this scenario, we use a geometry of the flexural faulting obtained from Li et al. (2017), where the flexural faults are subparallel to the bedding in the limb of the monocline and strike parallel to the fold axis. The fourth system is a nearly vertical fault with significant throw that is observed in unpublished, proprietary seismic data at approximately the location of the fold axis in the Hogback. The fifth system consists of faults mapped by Lorenz and Cooper (2001) that strike east-west in the Dakota sandstone within about twenty miles to the west of our proposed site. These faults may be too distant for significant pressurization, but they represent the type of faults of interest in the sedimentary column of the inner basin, and so by analyzing them, we can better understand the seismic risk of the region of interest. All told, these five fault systems give a varied view of strike, depth, and geology to investigate to elucidate the seismic hazard.

For our Mohr-Coulomb analyses, we recognize that none of the input parameters is certain. Therefore, to account for what is a large amount of uncertainty over eight input parameters (S_{Hmax} orientation, pore pressure, minimum horizontal stress, maximum horizontal stress, vertical stress, coefficient of friction, strike, and dip) we chose to use a Monte Carlo approach adapted from Walsh and Zoback (2016). By randomly sampling from a distribution for each input parameter with a sufficiently high number of realizations for each faulting scenario (~20,000), we can not only fully incorporate uncertainty in the analysis, but we can also characterize the uncertainty based on what is known about each variable i.e., we can adopt the ranges and distribution type appropriate for each variable. Table 1 summarizes the distributions of the inputs for each case. The standard deviations of the horizontal principal stresses represent 10% of the mean, and since the pore pressure and vertical stress are better constrained, their standard deviations represent 4% of the mean. We exclude the depth as an input parameter because it is already accounted for by the uncertainty in the stresses and pore pressure. The dip distribution for the vertical Hogback faulting scenario is a normal distribution centered at zero. This includes a 10-degree standard deviation, truncated only to allow for positive dip values because if it dips at all, it dips to the northwest. Based on formation tops compiled from wells throughout the basement, we use roughly 13,000 feet for the two basement scenarios, approximately 8,200 feet for the two Hogback scenarios, and roughly 7,100 for the Dakota scenario.

Parameter	Distribution type	Min/Mean	Max/Standard deviation
Taylor and Huffman (1998)			
Pore pressure	Normal	5,558 psi	222 psi
Min horiz. stress	Normal	9,230 psi	923 psi
Max horiz. stress	Normal	9,566 psi	957 psi
Vertical stress	Normal	14,634 psi	585 psi
Coeff. of friction	Normal	0.6	0.09
Strike	Normal	**35/125 degrees**	10 degrees
Dip	Uniform	0 degrees	90 degrees
S_{Hmax} orientation	Normal	35 degrees	10 degrees
Hogback Flexural			
Pore pressure	Normal	3,502 psi	140 psi
Min horiz. stress	Normal	5,242 psi	524 psi
Max horiz. Stress	Normal	5,580 psi	558 psi
Vertical stress	Normal	9,087 psi	363 psi

Coeff. of friction	Normal	0.6	0.09
Strike	Normal	45 degrees	10 degrees
Dip	Normal	50 degrees	10 degrees
S_{Hmax} orientation	Normal	35 degrees	10 degrees
Hogback vertical fault			
Pore pressure	Normal	3,502 psi	140 psi
Min horiz. stress	Normal	5,242 psi	524 psi
Max horiz. stress	Normal	5,580 psi	558 psi
Vertical stress	Normal	9,087 psi	363 psi
Coeff. of friction	Normal	0.6	0.09
Strike	Normal	225 degrees	10 degrees
Dip	Truncated Normal	0 degrees	10 degrees
S_{Hmax} orientation	Normal	35 degrees	10 degrees
Lorenz and Cooper (2001)			
Pore pressure	Normal	3,116 psi	125 psi
Min horiz. stress	Normal	4,813 psi	481 psi
Max horiz. stress	Normal	5,284 psi	528 psi
Vertical stress	Normal	8,083 psi	323 psi
Coeff. of friction	Normal	0.6	0.09
Strike	Normal	90 degrees	10 degrees
Dip	Uniform	0 degrees	90 degrees
S_{Hmax} orientation	Normal	35 degrees	10 degrees

Table 1: Input distributions for the five scenarios. The strike is bold in the first two scenarios because that is the sole difference between the two.

3 Results and Discussion

3.1 Primary Findings

Results suggest that the most uncertain parameter is the dip (Table 1) because this attribute is commonly neglected in geological characterizations of the San Juan Basin faults. Figure 4 shows a representation of twenty realizations for each faulting scenario using the distributions in Table 1. In this figure, the state of stress for all five scenarios is close to critically stressed, i.e., the Mohr circles are nearly touching the failure envelopes, especially when taking the mean values (dark lines) of the Hogback and Dakota analyses into account, which agrees with what was shown in the frictional equilibrium line of Figure 3. Also apparent in these figures is the effect of depth. The basement faults have greater stresses than the Hogback, which has greater stresses than the Dakota simply as a result of being deeper in the sedimentary column and increasing the overburden. The two basement cases are nearly indistinguishable given the radial normal faulting regime of the San Juan Basin.

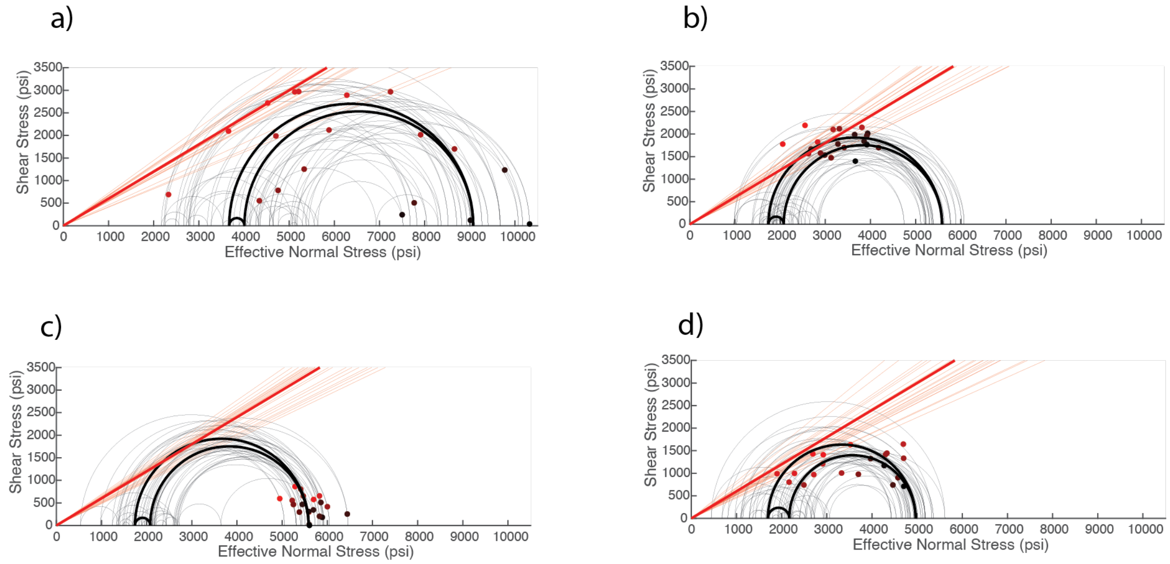

Figure 4: Probabilistic Mohr circles for twenty realizations for each of the fault scenarios using a standard deviation given in Table 1; this is the error value assumed for the subsequent analyses. The dark lines indicate the mean values of principal stresses, pore pressure, and coefficient of friction. The colors of the fault planes represent their Coulomb failure function (This is relative to the failure envelope of that particular realization). Twenty realizations were chosen for ease of visualization. a) The basement fault case of Taylor and Huffman (1998) with a strike of 35 degrees. The case with a strike of 125 degrees is not shown, but closely resembles the 35-degree case. b) Hogback flexural faulting case. c) Hogback vertical faulting case. d) Dakota Sandstone faults published in Lorenz and Cooper (2001).

To assess the uncertainty fully, it is necessary to evaluate the entire suite of 20,000 Monte Carlo simulations per faulting scenario. Figure 5 consists of a box plot of the Coulomb failure function (CFF) for each of the five scenarios. As expected (Figure 4), the basement faults are further from the failure envelope and the two shallower scenarios are closer. While there are some realizations for all five scenarios that exhibit a positive Coulomb failure function – i.e. they are likely to slip – the overwhelming majority of realizations (87.3%) have negative Coulomb failure functions, so the stresses resolved on the fault plane are not critical. The mean Coulomb failure function for the basement strike of 35 degrees, basement strike of 125 degrees, the Hogback flexural faults, the Hogback vertical fault, and the Dakota faults respectively are -1,897 psi, -2,484 psi, -120 psi, -2,755, and -1,132 psi (Figure 5). This means that the pore pressure or stress perturbation from injection of carbon dioxide is expected to trigger earthquakes only when these values are exceeded. At the stratigraphic characterization well, the closest well to the injection wells, the maximum pore pressure perturbation forecasted by from numerical modeling results is roughly 400 psi (the lighter dashed horizontal line in Figure 5). Thus, the flexural faults in the Hogback have the highest CFF distribution values of the five faulting scenarios.

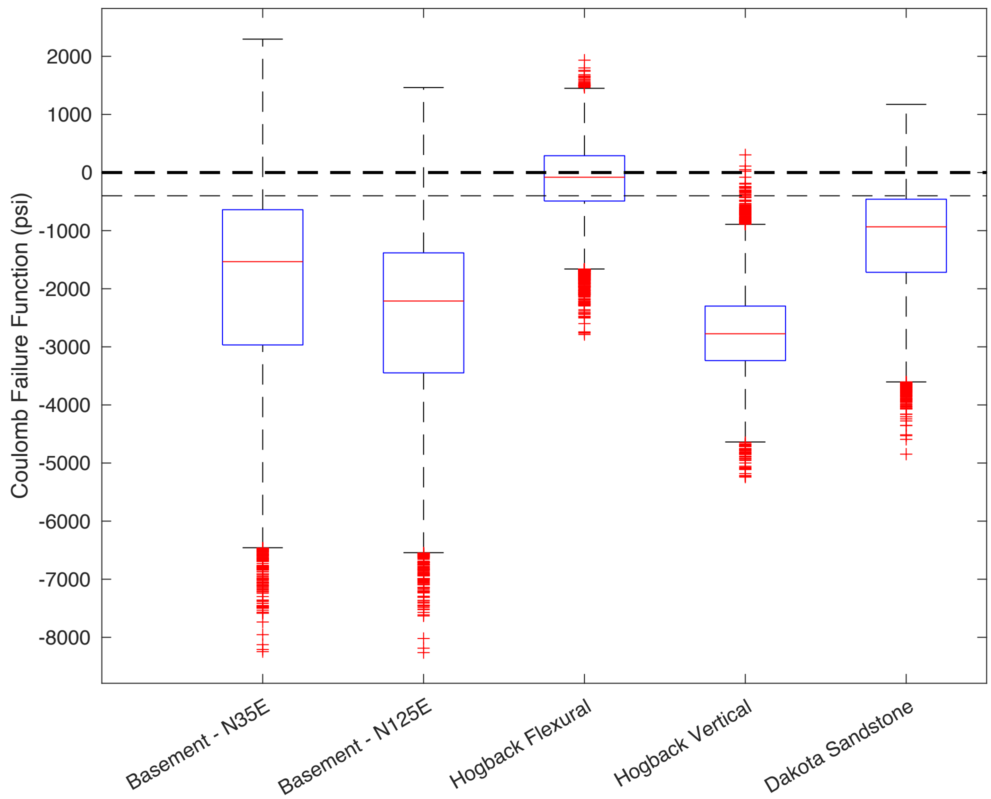

Figure 5: Box plots of the 20,000 realizations for each of the five scenarios. The darker dashed black line represents the frictional faulting equilibrium line (CFF = 0 psi). The lighter dashed black line is the expected maximum pore pressure perturbation (CFF = -400 psi).

By observing the sensitivities of the input parameters in addition to the aggregated outputs, we can suggest which parameters have the greatest impact on the CFF. We assembled sensitivity plots or tornado diagrams for each of the input parameters in each of the faulting scenarios (Figure 6) except for the basement faults striking 125 degrees because that case is highly similar to the basement faults striking 35 degrees. For these plots, each parameter was calculated for a high and a low value based on the distributions in Table 1 while all of the other parameters were held at the mean value. The Coulomb failure function using the mean value of all the parameters differs from the mean of the 20,000 realizations for each faulting scenario, because the sensitivity to the dip is so high. Changing the dip serves predominantly to lower the CFF (Figure 6) – certainly at the extremes of 0-degree dip and 90-degree dip in a normal faulting stress regime. Given its normal distribution of the dip (rather than the uniform and truncated normal for the other four scenarios), the Hogback flexural scenario potential is less dependent on the dip. Also, all five scenarios exhibit a strong dependence on the coefficient of friction both at low and high values of the coefficient of friction. The strike and the S_{Hmax} orientation had little influence on the resulting CFF. We already postulated that the strike would be of little impact, but the S_{Hmax} orientation has a similar geomechanical influence on the faulting scenarios as the strike due to the radial normal faulting. That is, the S_{Hmax} orientation is of minor impact because the S_{Hmax} and S_{hmin} are so similar, and a rotation of the stresses causes only a small change geomechanically. The CFF exhibits a minor dependence on the three principal stresses and pore pressure, albeit this dependence is more pronounced in certain scenarios.

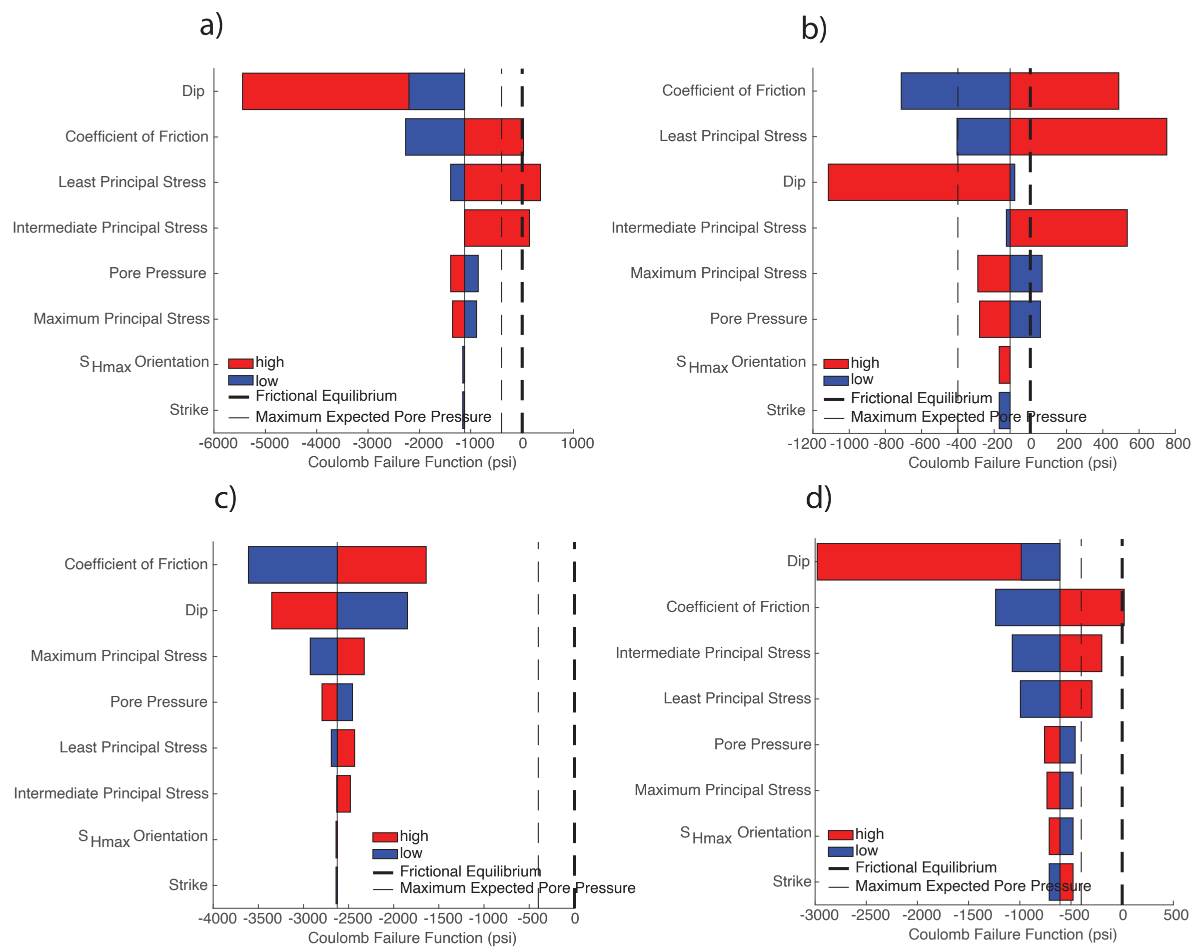

Figure 6: Sensitivity plots of four of the five faulting scenarios. a) The basement fault case of Taylor and Huffman (1998) with a strike of 35 degrees. The case with a strike of 125 degrees is not shown, but closely resembles the 35-degree case. b) Hogback flexural faulting case. c) Hogback vertical faulting case. d) Dakota Sandstone faults published in Lorenz and Cooper (2001). The red bars represent the sensitivity to increasing the parameter from the mean value, and the blue bars represent the sensitivity to decreasing the parameter from the mean value. The darker dashed black line represents the frictional faulting equilibrium line (CFF = 0 psi). The lighter dashed black line is the expected maximum pore pressure perturbation (CFF = -400 psi).

3.2 Key Interpretations

Mohr-Coulomb analyses are necessarily conservative for three reasons. One, there will only be slip on a well-oriented fault if such a fault is actually present. Two, if that fault is present and does slip, it will only be a large earthquake if the area of rupture is large. And three, the stresses resolved on a fault may not be the far-field stresses (Figure 3). If a fault has slipped in the recent geologic past, a static stress drop will have reduced the shear stress resolved on the fault plane, suggesting that the true Coulomb failure function is less than the Coulomb failure function calculated here.

We suggest that this conservative analysis of the Hogback flexural faults – and indeed all five scenarios – corresponds to a worst-case scenario. Because there is little detected background seismicity on the Hogback, we interpret that displacement on the limb of the monocline through the movement of the flexural faults is distributed across a series of faults parallel to many different bedding planes, such that predominantly small events occur. Therefore, we do not anticipate any one large fault with high hazard, but rather a series of smaller faults that distribute the seismicity between them.

It is possible that additional seismicity has gone undetected in the Hogback. Indeed, the two earthquakes detected along the Hogback in the region of interest (Figure 1) were detected during the two-year period that the USArray was in place. Also, there are two saltwater disposal wells in the Hogback and within five miles of the area of interest that have been operational for decades with injection into the Entrada and the shallower Bluff formations. These wells injected over twenty million barrels of water during their operational lifetimes, and yet we speculate that the two detected seismic events in the Hogback during that time were not induced: they are about a mile away from the closer injector, and the hypocenters were about 2,000 feet shallower than the injection interval for the larger event and about 4,500 feet shallower for the smaller event. The entire San Juan Basin CarbonSAFE storage complex resides between the injection interval and the hypocenters. These saltwater disposal wells effectively conducted a pressurization experiment on the Hogback and found negligible risk, i.e., no large earthquakes to date. We interpret the lack of appreciable seismicity along the Hogback monocline in the recorded past is because the flexural faults are producing small, mostly undetectable, events. We do expect the injection of the supercritical carbon dioxide to cause seismicity in the Hogback, but we expect these events to be of small magnitude in the same manner as those hypothesized from the saltwater disposal.

5 Conclusions

1. Five faulting scenarios were tested in the San Juan Basin for their ability to cause a medium- to large-scale rupture. Probabilistic geomechanical simulations showed that the Coulomb failure functions of the two basement scenarios, the Hogback vertical fault scenario, and the Dakota sandstone scenario are unlikely to induce earthquakes. The Hogback monocline flexural faulting scenario, however, has a relatively high distribution of CFFs, which means that this scenario could potentially induce earthquakes, but by analyzing the geologic and past seismological context as well as the past saltwater disposal, we expect small events, not large events on this series of faults.
2. For all five scenarios, we observed that the sensitivity of the CFF distributions to the S_{Hmax} orientation and the strike of the faults was minimal. Conversely, the sensitivity to the dip and the coefficient of friction was significant. Furthermore, varying the dip served to decrease the Coulomb failure functions in nearly every case, which is why the mean of the distributions of the CFFs is less than the CFF calculated using solely the mean values.
3. Finally, assessing seismic risk to absolute certainty is impossible. There can always be additional, complicating factors, or information that was inadvertently omitted from the analysis. Thus, we conducted a scientific analysis on the potential for induced seismicity associated with the San Juan Basin CarbonSAFE Phase III project, and we have found the risk of a sizeable earthquake to be appreciably small. The expected lack of large seismic rupture does not mean, however, that a damaging event cannot happen.

Acknowledgments

This material is based upon work supported by the Department of Energy under Award Number DE-FE0031890 as part of the San Juan Basin CarbonSAFE project. We would also like to acknowledge Nathan Moodie for his numerical modeling work and Rich Esser for his contributions to Figure 1. Also, Dana Ulmer-Scholle and Luke Martin provided invaluable data from logs and geological sources. Finally, the entire San Juan Basin CarbonSAFE project team's great scientific efforts have made this work possible.

Open Research

The data used in this paper (Table 1) comes from information in published literature on the San Juan Basin and petrophysical data in wells nearby the proposed injection site. The petrophysical data can be found at the New Mexico Oil Conservatoin website (New Mexico, 2021), and the literature regarding the faulting parameters has been cited thoroughly in the Methodology section. The geomechanical simulation MATLB code can be found at Github (McCormack, 2021), and the petrophysical software is named Techlog version 2121.1.1 (it requires a license). Finally, the regional seismicity data sources used to make Figure 1 is cited in the text.

References

Astiz, L. et al. 2014. "The Array Network Facility Seismic Bulletin: Products and an Unbiased View of United States Seismicity", *Seismol. Res. Lett., 85*, 576-593

Bratton, T. and Soroka, M., "Improved Vertical Stress Profiling for Unconventional Reservoirs", First Break, Vol. 26, July 2018.

Catalli, Flaminia, Antonio P. Rinaldi, Valentin Gischig, Massimo Nespoli, and Stefan Wiemer. 2016. "The Importance of Earthquake Interactions for Injection-Induced Seismicity: Retrospective Modeling of the Basel Enhanced Geothermal System." *Geophysical Research Letters* 43 (10): 4992–99. https://doi.org/10.1002/2016GL068932.

Craigg, S. 2001. “Geologic framework of the San Juan structural basin of New Mexico, Colorado, Arizona, and Utah, with emphasis on Triassic through Tertiary rocks.” *U.S. Geological Survey Professional Paper*. Number 1420.

Coates, G. and Denoo, S., “Mechanical Properties Program using Borehole Analysis and Mohr’s Circle”, SPWLA Twenty-Second Annual Logging Symposium, Paper DD, June 23-26, 1981.

Dart, S. 1992. “Evaluation of San Juan Basin fractured reservoirs from surface data.” *The Rocky Mountain Association of Geologists.* Pages: 95-114.

Davies, Richard, Gillian Foulger, Annette Bindley, and Peter Styles. 2013. “Induced Seismicity and Hydraulic Fracturing for the Recovery of Hydrocarbons.” *Marine and Petroleum Geology* 45: 171–85. https://doi.org/10.1016/j.marpetgeo.2013.03.016.

Ellsworth, William L., Domenico Giardini, John Townend, Shemin Ge, and Toshihiko Shimamoto. 2019. “Triggering of the Pohang, Korea, Earthquake (Mw 5.5) by Enhanced Geothermal System Stimulation.” *Seismological Research Letters* 90 (5): 1844–58. https://doi.org/10.1785/0220190102.

Fassett, J. and Boyce, B. 2005. “Fractured-sandstone gas reservoirs, San Juan Basin, New Mexico and Colorado: Stratigraphic traps, not basin centered gas deposits – With an overview of Fruitland Formation coal-bed methane.” *The Rocky Mountain Association of Geologists.* Pages: 109-185.

Gorham, F., Woodward, L., Callender, J., and Greer, A. 1979. “Fractures in Cretaceous rocks from selected areas of San Juan Basin, New Mexico – Exploration implications.” *The American Assocciation of Petroleum Geologists Bulletin*. Vol. 63, No. 4, p. 598-607.

Grigoli, F, S Cesca, A P Rinaldi, A Manconi, J F Clinton, R Westaway, C Cauzzi, T Dahm, and S Wiemer. 2018. “The November 2017 Mw 5.5 Pohang Earthquake: A Possible Case of Induced Seismicity in South Korea” 5 (June): 1003–6.

Hart, B. and Cooper, S. 2021. “Mechanical stratigraphy in Mesozoic rocks of the San Juan Basin: Integration stratigraphic and structural terms and concepts.” *The Mountain Geologist.* Vol. 58, No. 2, Pp. 159-204.

Herron, M., “Estimating the Intrinsic Permeability of Clastic Sediments from Geochemical Data”, SPWLA Twenty-Eighth Annual Logging Symposium, Paper HH, June 29-July 2, 1987.

Herron, M., Herron, S., and Plumb, R., “Identification of Clay-Supported and Framework-Supported Domains from Geochemical and Geophysical Well Log Data”, SPE 24726, 1992.

Kelley, Vincent C. 1957. "Tectonics of the San Juan Basin and Surrounding Areas." *Four Corners Geological Society Guidebook.*

Krevor, Samuel C.M., Ronny Pini, Lin Zuo, and Sally M. Benson. 2012. "Relative Permeability and Trapping of CO_2 and Water in Sandstone Rocks at Reservoir Conditions." *Water Resources Research* 48 (2): 1–16. https://doi.org/10.1029/2011WR010859.

Langenbruch, Cornelius, and Mark D. Zoback. 2017. "Response to Comment on 'How Will Induced Seismicity in Oklahoma Respond to Decreased Saltwater Injection Rates?'" *Science Advances* 3 (8): 1–10. https://doi.org/10.1126/sciadv.aao2277.

Li, Tao, Jie Chen, Jessica A. Thompson Jobe, and Douglas W. Burbank. 2017. "Active Flexural-Slip Faulting: Controls Exerted by Stratigraphy, Geometry, and Fold Kinematics." *Journal of Geophysical Research: Solid Earth* 122 (10): 8538–65. https://doi.org/10.1002/2017JB013966.

Lorenz, J. and Cooper, S. 2001. "Tectonic setting and characteristics of natural fractures in Mesaverde and Dakota reservoirs of the San Juan Basin, New Mexico and Colorado." *Sandia National Laboratories: Project Report.*

Lorenz, J. and Cooper, S. 2003. "Tectonic setting and characteristics of natural fractures in Mesaverde and Dakota reservoirs of the San Juan Basin." *New Mexico Geology.* Vol. 25. Issue 1.

Lund Snee, Jens-Erik, and Mark D Zoback. 2020. "Multiscale Variations of the Crustal Stress Field throughout North America." *Nature Communications*, no. 1951: 1–9. https://doi.org/10.1038/s41467-020-15841-5.

Majer, E. et al. 2004. "A handbook for the application of seismic methods for quantifying naturally fractured gas reservoirs in the San Juan Basin, New Mexico." *National Energy Technology Laboratory: Project Report.*

Majer, Ernest L., Roy Baria, Mitch Stark, Stephen Oates, Julian Bommer, Bill Smith, and Hiroshi Asanuma. 2007. "Induced Seismicity Associated with Enhanced Geothermal Systems." *Geothermics* 36 (3): 185–222. https://doi.org/10.1016/j.geothermics.2007.03.003.

Mazzoldi, Alberto, Antonio P. Rinaldi, Andrea Borgia, and Jonny Rutqvist. 2012. "Induced Seismicity within Geological Carbon Sequestration Projects: Maximum Earthquake Magnitude and Leakage Potential from Undetected Faults." *International Journal of Greenhouse Gas Control* 10: 434–42. https://doi.org/10.1016/j.ijggc.2012.07.012.

McClure, Mark W., and Roland N. Horne. 2011. "Investigation of Injection-Induced Seismicity Using a Coupled Fluid Flow and Rate/State Friction Model." *Geophysics* 76 (6). https://doi.org/10.1190/geo2011-0064.1.

McCormack, Kevin L. 2021. Probabibalistic assessment of faulting data. *Github*. https://github.com/kvnmccrmck/JGR2021

Mignan, A., D. Landtwing, P. Kästli, B. Mena, and S. Wiemer. 2015. "Induced Seismicity Risk Analysis of the 2006 Basel, Switzerland, Enhanced Geothermal System Project: Influence of Uncertainties on Risk Mitigation." *Geothermics* 53: 133–46. https://doi.org/10.1016/j.geothermics.2014.05.007.

Morales, R.H., Marcinew, R.P., Dowell, S. 1993. "Fracturing of high-permeability formations: Mechanical properties correlations." *SPE Extended Abstracts*.

New Mexico Oil Conservation Division. 2021. Well File Search. https://ocdimage.emnrd.state.nm.us/imaging/

Nicol, A., R. Carne, M. Gerstenberger, and A. Christophersen. 2011. "Induced Seismicity and Its Implications for CO2 Storage Risk." *Energy Procedia* 4: 3699–3706. https://doi.org/10.1016/j.egypro.2011.02.302.

Plumb, R., "Influence of Composition and Texture on the Failure Properties of Clastic Rocks", Eurock 94, Balkema, Rotterdam, 1994.

Pursley, J.; Bilek, S. L. & Ruhl, C. J. 2013. "Earthquake catalogs for New Mexico and bordering areas: 2005—2009." *New Mexico Geology, 35*.

Rubinstein, Justin L., and Alireza Babaie Mahani. 2015. "Myths and Facts on Wastewater Injection, Hydraulic Fracturing, Enhanced Oil Recovery, and Induced Seismicity." *Seismological Research Letters* 86 (4): 1060–67. https://doi.org/10.1785/0220150067.

Rutqvist, Jonny, Antonio P. Rinaldi, Frederic Cappa, Pierre Jeanne, Alberto Mazzoldi, Luca Urpi, Yves Guglielmi, and Victor Vilarrasa. 2016. "Fault Activation and Induced Seismicity in Geological Carbon Storage – Lessons Learned from Recent Modeling Studies." *Journal of Rock Mechanics and Geotechnical Engineering* 8 (6): 789–804. https://doi.org/10.1016/j.jrmge.2016.09.001.

Sanford, A. R.; Olsen, K. H. & Jaksha, L. H. 1981. "Earthquakes in New Mexico, 1849-1977." *New Mexico Bureau of Mines & Mineral Resources.*

Sanford, A. R.; Lin, K. W..; Tsai, I. C. & Jaksha, L. H. 2002. "Earthquake catalogs for New Mexico and bordering areas: 1869—1998." *New Mexico Bureau of Geology and Mineral Resources Circular, 210.*

Sanford, A. R.; Mayeau, T. M.; Schlue, J. W.; Aster, R. C. & Jaksha, L. H. 2006. "Earthquake catalogs for New Mexico and bordering areas II: 1999—2004." *New Mexico Bureau of Geology and Mineral Resources Circular, 28*, 99-109.

Schultz, R., G. Atkinson, D. W. Eaton, Y. J. Gu, and H. Kao. 2018. "Hydraulic Fracturing Volume Is Associated with Induced Earthquake Productivity in the Duvernay Play." *Science* 359 (6373): 304–8. https://doi.org/10.1126/science.aao0159.

Shapiro, S. A., and C. Dinske. 2009. "Fluid-Induced Seismicity: Pressure Diffusion and Hydraulic Fracturing." *Geophysical Prospecting* 57 (2): 301–10. https://doi.org/10.1111/j.1365-2478.2008.00770.x.

Taylor, D. and Huffman, C. 1998. "Map showing inferred and mapped basement faults, San Juan Basin and vicinity, New Mexico and Colorado." *USGS Publication.* Geologic Investigations Series.

Torp, Tore A., and John Gale. 2004. "Demonstrating Storage of CO2 in Geological Reservoirs: The Sleipner and SACS Projects." *Energy* 29 (9–10): 1361–69. https://doi.org/10.1016/j.energy.2004.03.104.

Townend, J., and M. D. Zoback. 2000. "How Faulting Keeps the Crust Strong." *Geology* 28 (5): 399–402. https://doi.org/10.1130/0091-7613

Vilarrasa, Víctor, Jesus Carrera, Sebastià Olivella, Jonny Rutqvist, and Lyesse Laloui. 2019. "Induced Seismicity in Geologic Carbon Storage." *Solid Earth* 10 (3): 871–92. https://doi.org/10.5194/se-10-871-2019.

Walsh F. and Zoback, M. 2015. "Oklahoma's recent earthquakes and saltwater disposal." *Science Advances.* Vol. 1, Issue 5, Pages 1-9.

Walsh, F. Rall, and Mark D. Zoback. 2016. "Probabilistic Assessment of Potential Fault Slip Related to Injectioninduced Earthquakes: Application to North-Central Oklahoma, USA." *Geology* 44 (12): 991–94. https://doi.org/10.1130/G38275.1.

Warpinski, N. R., J. Du, and U. Zimmer. 2012. "Measurements of Hydraulic-Fracture-Induced Seismicity in Gas Shales." *SPE Production and Operations* 27 (3): 240–52. https://doi.org/10.2118/151597-PA.

White, Joshua A., and William Foxall. 2016. "Assessing Induced Seismicity Risk at CO2 Storage Projects: Recent Progress and Remaining Challenges." *International Journal of Greenhouse Gas Control* 49: 413–24. https://doi.org/10.1016/j.ijggc.2016.03.021.

Zoback, M. 2007. "Reservoir Geomechanics." *Cambridge University Press*.

Figure and Table Captions

Figure 1: Map of the seismicity from roughly 60 years of USGS instrumentation and a short period of local instrumentation. There are a total of 1091 events. The dark green outline is the Hogback Monocline as interpreted from Lorenz and Cooper (2003). The 30-045-30040 well corresponds to the primary well used to create the integrated earth model (below).

Figure 2: The components of an integrated earth model (inside the boxes) and typical sources of input data (outside of the boxes).

Figure 3: The stress profile obtained from the integrated earth model.

Table 1: Input distributions for the five scenarios. The strike is bold in the first two scenarios because that is the sole difference between the two.

Figure 4: Probabilistic Mohr circles for twenty realizations for each of the fault scenarios using a standard deviation given in Table 1; this is the error value assumed for the subsequent analyses. The dark lines indicate the mean values of principal stresses, pore pressure, and coefficient of friction. The colors of the fault planes represent their Coulomb failure function (This is relative to the failure envelope of that particular realization). Twenty realizations were chosen for ease of visualization. a) The basement fault case of Taylor and Huffman (1998) with a strike of 35 degrees. The case with a strike of 125 degrees is not shown, but closely resembles the 35-degree case. b) Hogback flexural faulting case. c) Hogback vertical faulting case. d) Dakota Sandstone faults published in Lorenz and Cooper (2001).

Figure 5: Box plots of the 20,000 realizations for each of the five scenarios. The darker dashed black line represents the frictional faulting equilibrium line (CFF = 0 psi). The lighter dashed black line is the expected maximum pore pressure perturbation (CFF = -400 psi).

Figure 6: Sensitivity plots of four of the five faulting scenarios. a) The basement fault case of Taylor and Huffman (1998) with a strike of 35 degrees. The case with a strike of 125 degrees is not shown, but closely resembles the 35-degree case. b) Hogback flexural faulting case. c) Hogback vertical faulting case. d) Dakota Sandstone faults published in Lorenz and Cooper (2001). The red bars represent the sensitivity to increasing the parameter from the mean value, and the blue bars represent the sensitivity to decreasing the parameter from the mean value. The darker dashed black line represents the frictional faulting equilibrium line (CFF = 0 psi). The lighter dashed black line is the expected maximum pore pressure perturbation (CFF = -400 psi).